



1 **WHICH RAINFALL METRIC IS MORE INFORMATIVE ABOUT THE**
2 **FLOOD SIMULATION PERFORMANCE? A COMPREHENSIVE**
3 **ASSESSMENT ON 1318 BASINS OVER EUROPE**

4 Stefania Camici ⁽¹⁾, Christian Massari ⁽¹⁾, Luca Ciabatta ⁽¹⁾, Ivan Marchesini ⁽¹⁾, Luca Brocca ⁽¹⁾

5 *(1) National Research Council, Research Institute for Geo-Hydrological Protection, Perugia, Italy (s.camici@irpi.cnr.it)*

6

7

8

9

10

11

12

13

14

15

16

17

18

19

20

* Correspondence to: Ph.D. Stefania Camici, Research Institute for Geo-Hydrological Protection, National Research Council, Via della Madonna Alta 126, 06128 Perugia, Italy. Tel: +39 0755014419 Fax: +39 0755014420 E-mail: stefania.camici@irpi.cnr.it.



22 **ABSTRACT**

23 The global availability of satellite rainfall products (SRPs) at an increasingly high temporal/spatial
24 resolution has made possible their exploitation in hydrological applications, especially over in-situ
25 data scarce regions. In this context, understand how uncertainties transfer from SRPs into flood
26 simulation, through the hydrological model, is a main research question.

27 SRPs accuracy is normally characterized by comparing them with ground observations via the
28 calculation of categorical (e.g., threat score, false alarm ratio, probability of detection) and/or
29 continuous (e.g., bias, root mean square error, Nash-Sutcliffe index, Kling-Gupta efficiency index,
30 correlation coefficient) metrics. However, whether these metrics are informative about the
31 associated performance in flood simulations (when the SRP is used as input to an hydrological
32 model) is an underdiscussed research topic.

33 This study aims to relate the accuracy of different SRPs both in terms of rainfall and in terms of
34 flood simulation. That is, the following research question are addressed: is (are) there appropriate
35 performance metric (s) to drive the choice of the best performing rainfall product for flood
36 simulation? To answer this question three SRPs, namely the Tropical Rainfall Measurement
37 Mission Multi-satellite Precipitation Analysis, TMPA; the Climate Prediction Center Morphing
38 algorithm, CMORPH, and the SM2RAIN algorithm applied to the ASCAT (Advanced
39 SCATterometer) soil moisture product, SM2RAIN-ASCAT, have been used as input into a lumped
40 hydrologic model (MISDc, “Modello Idrologico Semi-Distribuito in continuo”) on 1318 basins
41 over Europe with different physiographic characteristics.

42 Results have suggested that, among the continuous metrics, correlation coefficient and Kling-Gupta
43 efficiency index are not reliable scores to select rainfall product performing best for hydrological
44 modelling whereas bias and root mean square error seem more appropriate. In particular, by
45 constraining the relative bias to values lower than 0.2 and the relative root mean square error to
46 values lower than 2, good hydrological performances (Kling-Gupta efficiency index on discharge



47 greater than 0.5) are ensured for almost 75% of the basins fulfilling these criteria. Conversely, the
48 categorical scores have not provided suitable information to address the SRPs selection for
49 hydrological modelling.

50

51 Key words: satellite rainfall products, hydrological validation, rainfall-runoff modelling, Europe.

52 1. INTRODUCTION

53 Accurate rainfall estimate is essential in many fields spanning from climate change research,
54 weather prediction and hydrologic applications (Tapiador et al., 2017, Ricciardelli et al., 2018, Lu et
55 al., 2018). In particular, the delivery of real time rainfall observations is one of the most challenging
56 task in operational flood forecasting both for technical reasons related to the need of a prompt
57 release of the observations and for scientific motives linked to the necessity of ensuring sufficient
58 accuracy to provide a reliable forecasting. Generally rainfall observations are obtained through real
59 time ground monitoring networks (e.g., Artan et al., 2007), meteorological and numerical weather
60 prediction models (e.g. Montani et al., 2011; Zappa et al., 2008) and, more recently, by satellite
61 observations (Mugnai et al., 2013) that, albeit with some difficulties (Maggioni and Massari, 2018)
62 are gaining ground with respect to the classical rainfall monitoring methods.

63 The global availability of near real time satellite rainfall products (SRPs) has boost their use for
64 hydrological applications, specifically for river discharge estimation via rainfall-runoff models
65 (Casse et al., 2015; Elgamal et al., 2017; Camici et al., 2018; Beck et al., 2017, see Maggioni and
66 Massari, 2018 and Jiang and Wang, 2019 for a more complete review). In particular, in the past
67 decade a special attention has been paid on the propagation of the satellite rainfall error on flood
68 simulations (Hong et al., 2006; Hossain, and Anagnostou, 2006; Pan et al., 2010; Maggioni et al.
69 2013; Thiemig et al. 2013; Bhuiyan et al., 2019) and two approaches, one probabilistic and one
70 statistical, can be recognized (Quintero et al., 2016). In the probabilistic approach a statistical model
71 is first used to produce an ensemble of possible rainfall realizations. Then, each rainfall realization



72 is used to simulate discharge time series through an hydrologic model and the difference between
73 simulated and in situ discharge data is used to assess how rainfall accuracy transfers to the flood
74 simulation (e.g., Hong et al., 2006; Hossain, and Anagnostou, 2006; Demaria et al. 2014; Maggioni
75 et al. 2013, 2011). In the deterministic approach, SRPs are first compared with a reference dataset to
76 assess the accuracy in terms of rainfall estimate. Then, SRPs are used as input in rainfall-runoff
77 models to estimate river discharge that is then compared with in situ discharge observations.
78 Eventually, the existence and the shape of the relationship between the SPR accuracy and the
79 associated discharge score is analysed (e.g., Serpetzoglou et al. 2010; Pan et al., 2010; Thiemig et al.
80 2013; Chintalapudi et al. 2014; Pakoksung and Takagi, 2016; Shah and Mishra, 2016; Qi et al.
81 2016; Ren et al., 2018; Bhuiyan et al., 2019).

82 In both approaches, several continuous (e.g., bias, root mean square error, RMSE, correlation
83 coefficient, R, Nash-Sutcliffe efficiency index, NSE, Kling-Gupta efficiency index, KGE) and
84 categorical (e.g., probability of detection, POD, false alarm ratio, FAR, threat score, TS)
85 performance scores are used to characterize the accuracy in terms of rainfall and river discharge.
86 Generally this comparison has been carried out for few basins (e.g., Hong et al., 2006; Pan et al.,
87 2010; Demaria et al., 2014; Chintalapudi et al., 2014; Qi et al. 2016; Ren et al., 2018; Thiemig et al.
88 2013), rarely at regional scale (e.g., Bhuiyan et al., 2019), whereas no studies investigated the
89 hydrological propagation of SRP error at a continental scale. In Beck et al (2017), the authors
90 carried out an evaluation of multiple (22) global daily rainfall datasets both in terms of rainfall and
91 discharge for many (+9000) basins over the globe, however, the relationship between the accuracy
92 in terms of rainfall and discharge was not investigated in detail.

93 From both the probabilistic and the statistical approach, arises that the hydrological performances of
94 SRPs depend on a complex interaction among the characteristics of the input data (i.e., precipitation
95 type, seasonality, data resolution or time window considered, see e.g., Ebert et al., 2007; Vergara et
96 al., 2014; Satgé et al., 2019), the hydrological model formulation (i.e. parameter estimation and
97 modelled processes, Quintero et al., 2016; Mei et al., 2017; Bhuiyan et al., 2019), the characteristics



98 of the basin (e.g., area and initial soil moisture conditions, land use and land cover Yong et al.,
99 2010; Yilmaz et al., 2005; Nikolopoulos et al., 2010; Mei et al., 2016; Shah and Mishra, 2016;
100 Gebregiorgis et al., 2012) and observations (i.e., streamflow data, see e.g., Nikolopoulos et al.,
101 2012). In this context, it is not trivial to draw general guidelines about which SRPs should be
102 favoured or which error metric(s) should be used to identify the best performing rainfall product for
103 flood forecasting (Qi et al., 2016; Hossain and Huffman, 2008). The only largely accepted
104 suggestion is about SRP bias, recognized as a major issue for a reliable flood forecast across several
105 basins around the world (Maggioni et al., 2013; Thiemig et al. 2013; Shah and Mishra 2016; Jiang
106 and Wang, 2019). Based on that, bias correction methods have shown to significantly reduce
107 streamflow errors (e. g, Yilmaz et al. 2005; Bitew et al., 2012; Valdes-Pined et al., 2016). For
108 instance, by using MIKE SHE model on a small and mountainous basin in the Blue Nile basin,
109 Bitew et al. (2012) stated that large biases in satellite rainfall directly translate into bias in one or
110 more of the hydrology simulation components. Zhu et al. (2016) found that for two humid basins in
111 China, the accuracy on flood simulations is related to the mean error and to bias in the rainfall
112 estimates as also found by Yilmaz et al. (2005). Besides bias, it is difficult to found literature
113 studies advising on rainfall error metrics able to indicate flood simulation performances. The work
114 of Bisselink et al. (2016), even if conducted over only 4 basins in south Africa, is an exception. The
115 authors, by using different SRPs as input to LISFLOOD model, proved that a high correlation
116 between monthly rainfall and observed streamflow is a needed prerequisite for obtaining good
117 hydrological performances, as long as the rainfall variability in time is not too high.

118 Based on that, there is a need to investigate metrics that can more effectively advance the use of
119 SRPs for hydrological applications, and specifically for flood modelling at regional scales. This
120 paper aims to explore the link between satellite rainfall accuracy of different products and their
121 flood modelling performance. The following research questions are addressed: which is the most
122 appropriate performance metric to be used to select the best performing satellite rainfall product for



123 flood modelling? Are R and RMSE, generally used to characterize the rainfall accuracy,
124 informative about the hydrological modelling performance?
125 In pursuing this goal, three different near real time SRPs are considered, i.e., Tropical Rainfall
126 Measurement Mission (TRMM) Multi-satellite Precipitation Analysis (TMPA) real time product
127 (TMPA 3B42RT, Huffman et al., 2010), the Climate Prediction Center (CPC) morphing technique
128 (CMORPH, Joyce et al., 2004) and SM2RAIN-ASCAT rainfall product (Brocca et al., 2019)
129 obtained by applying the SM2RAIN algorithm (Brocca et al., 2014) to the ASCAT satellite soil
130 moisture product are used to force a lumped hydrological model, MISDc (Brocca et al., 2011) over
131 1318 basins spread out over Europe. An intercomparison of SRPs with respect to a benchmark
132 rainfall dataset, i.e., E-OBS (Haylock et al., 2008), is carried out. This step, along with the
133 reliability assessment of the different SRPs for flood modelling over Europe, constitutes only an
134 intermediate output of the work. The ultimate aim of the paper is to investigate how SRPs accuracy
135 propagates through the river discharge simulations, as to help in the selection of the rainfall metrics
136 more informative of better hydrological performances. As the intent of the paper is to analyse the
137 performances of near-real time satellite rainfall products, gauge-corrected satellite or reanalysis
138 rainfall products are not considered in this work.

139 2. STUDY AREA

140 The study area is composed by 1318 basins belonging to 23 different countries and spread over the
141 whole Europe, over longitude varying from -10° to 25° and latitude from 35° to 70° (Figure 1).
142 European continent is characterized by a complex topography ranging, from south to north, from
143 huge mountains towards hilly plateaus to a large plain. The Alpine mountain chain, crossing the
144 continent from west to east represents the highest and more extensive mountain range system in
145 Europe. Hilly plateaus gently slopes towards the Great European Plain, a low flat region, extending
146 from the Atlantic coast of France to the Urals, crossed by many rivers and with densely populated
147 cities.



148 The climate is humid continental with cold summers in central and eastern Europe. Mean annual
149 rainfall across Europe ranges between 300 mm year⁻¹ and 4000 mm year⁻¹, depending on the
150 location. The area east, west and north of the Alps generally is interested by higher rainfall amount,
151 while along the edges of the Mediterranean Sea and in northern Scandinavia, lighter rainfall is
152 common. In terms of floods, their occurrence range from spring to summer moving from
153 northeastern Europe towards the Alps, whereas Mediterranean region and western Europe are
154 prevailing subject to winter floods (Berghuijs et al., 2019).

155 The main features of the study basins, clustered according the latitude of the outlet section, are
156 summarized in Table 1: among the 1318 basins, more than half (889) have the outlet section located
157 below the 50° latitude and about 11% of them the outlet section is placed above 60° latitude. Basin
158 areas range in size from 200 to 136'000 km² and the median area of the basins located below 50° is
159 lower than the one of basins located in northern part of Europe (above 50° latitude). By considering
160 these features, the selected set of basins can be considered a comprehensive sample of the European
161 basin characteristics, definitely.

162 3. DATASETS

163 The datasets used in this study include both ground observations and satellite rainfall products
164 (Table 2).

165 3.1 Ground observations

166 Ground observations comprise rainfall, air temperature and river discharge data. Rainfall and air
167 temperature are extracted from the European high-resolution gridded data sets version 16.0 (E-OBS,
168 Haylock et al., 2008), currently maintained by the Copernicus Climate Change Service. The E-OBS
169 dataset is built using data from nearly 2316 stations (i.e., equivalent on average to a density of 1
170 stations every 4000 km²) but the station density significantly varies across Europe (see Haylock et
171 al., 2008; Cornes et al., 2018). However, as this product is composed by time series thoroughly
172 checked both in terms of quality and homogeneity (Klok and Tank, 2009) and it is continuously



173 available from 1950 up to now at daily time step, it can be considered a good benchmark for the
174 analysis.

175 Daily river discharge data are obtained through an european daily dataset, compiled by the authors
176 merging stations from 5 different databases: the Global Runoff Data Base (GRDC,
177 https://www.bafg.de/GRDC/EN/Home/homepage_node.html), the European Water Archive (EWA,
178 https://www.bafg.de/GRDC/EN/04_spcldtbss/42_EWA/ewa.html?nn=201574), the Italian ISPRA
179 HIS national database (<http://www.hiscentral.isprambiente.gov.it/hiscentral/default.aspx>); the
180 Portuguese national database (<http://snirh.pt/>) and the Spanish national database (<http://ceh-flumen64.cedex.es/anuarioaforos/default.asp>). From the resulting European dataset, composed by
181 3913 quality checked stations covering the period 1900-2016, 1318 stations with available
182 observations after 2007 (according the availability of SRPs, see paragraph 3.2) have been extracted.
183 The authors, using the EU-DEM digital elevation model (Mouratidis and Ampatzidis, 2019)
184 resampled at 100m ground resolution, developed an automatic and rapid procedure to delineate the
185 drainage watersheds located upstream of each discharge measurement location (outlet section). The
186 study basins and the related observation period length after 2007 is shown in Figure 1a: more than
187 50% of the basins have an observation period longer than 7 years; Spanish, Italian and Northern
188 European basins have a nearly complete observation period (10 years), whereas for Central Europe
189 some stations end the monitoring period on 2012 and the median length of discharge observations is
190 about 6/7 years (see Table 1).

192 **3.2 Satellite rainfall products**

193 Three different SRPs have been used in this study: TMPA 3B42RT, CMORPH and
194 SM2RAIN-ASCAT satellite products. As these products have been largely used in literature, only a
195 brief product description is reported in the following whereas for major details the reader is referred
196 to Huffman et al. (2010); Joyce et al. (2004) and Brocca et al. (2019) for TMPA 3B42RT,
197 CMORPH and SM2RAIN-ASCAT, respectively.



198 TMPA 3B42RT, provided by NASA (National Aeronautics and Space Administration,
199 <http://disc.sci.gsfc.nasa.gov/>) covers $\pm 50^\circ$ north-south latitude band with a spatial sampling of 0.25°
200 and a temporal resolution of 3 h from 1997 onward.

201 CMORPH is provided by CPC (Climate Prediction Center, <ftp://ftp.cpc.ncep.noaa.gov>) for the
202 $+60^\circ/-60^\circ$ latitude band from March 2000 up to now. In this study, the CMORPH raw version is
203 extracted with a spatial/temporal resolution of $0.25^\circ/3$ hours.

204 In addition to these state-of-the-art SRPs, we used the SM2RAIN-ASCAT rainfall product (Brocca
205 et al., 2019) obtained through the application of the SM2RAIN algorithm (Brocca et al., 2014) to
206 the ASCAT satellite soil moisture product (Wagner et al., 2013). SM2RAIN-ASCAT,
207 downloadable at <https://zenodo.org/record/3405563>, is available for the period 2007-2019, with a
208 12.5 km spatial sampling and a daily temporal aggregation.

209 For sake of simplicity, the TMPA 3B42RT, CMORPH and SM2RAIN-ASCAT satellite datasets are
210 indicated in the following as TMPA, CMOR and $SM2R_{ASCAT}$, respectively. By considering the
211 spatial/temporal availability of both ground-based and satellite observations (see Table 2 for a
212 summary), the analysis has been carried out to cover the maximum common observation period,
213 i.e., from 2007 to 2016 at daily time scale (TMPA and CMOR are aggregated at daily scale), with
214 three different areal masks cut: 1) at the original spatial coverage of each SRP, i.e., until 50° , 60°
215 and 70° latitude for TMPA, CMOR and $SM2R_{ASCAT}$, respectively; 2) below the TMPA area (latitude
216 $<50^\circ$); 3) above TMPA area (latitude $>50^\circ$).

217 4. METHOD

218 4.1 Hydrological model

219 The model applied to carried out the flood simulation is MISDc (“Modello Idrologico Semi-
220 Distribuito in continuo” Brocca et al. 2011), a two-layer continuous hydrological model composed
221 by a component simulating the temporal pattern of soil moisture and by a rainfall-runoff model
222 simulating flood. By using as input daily rainfall and air temperature data, MISDc simulates the



223 most important processes involved in the rainfall-runoff transformation (e.g., infiltration,
224 evapotranspiration, saturation excess and percolation). The geomorphological Instantaneous Unit
225 Hydrograph (IUH) is used to transfer surface and subsurface runoff to the outlet of the catchment.
226 The model (downloadable at: <http://hydrology.irpi.cnr.it/download-area/midsc-code/>) uses 9
227 parameters calibrated by maximizing the Kling-Gupta efficiency index (KGE, Gupta et al., 2009;
228 Kling et al., 2012, see paragraph 4.5 for more details) between observed and simulated river
229 discharge.

230 The successful results obtained through MISDc model for flood simulation in many different basins
231 (in Italy, see e.g., Brocca et al., 2011; 2013a, Massari et al. 2015; Masseroni et al. 2016; Cislaghi et
232 al. 2019, and in Europe, see e.g., Brocca et al., 2013b; Massari et al. 2018; Camici et al., 2018) and
233 for different applications (e.g., climate change impact studies, see Camici et al., 2014) allow to
234 consider the model suitable for the analysis purpose.

235 **4.2 Experimental design**

236 The first step of the analysis concerned on the quality assessment of the SRPs in terms of rainfall.
237 For that, each SRP has been compared with the daily E-OBS data used as reference. Then,
238 discharge simulations have been performed by running the lumped version of MISDc model with E-
239 OBS dataset (river discharge reference) and with each SRP as input. Specifically, the two following
240 steps have been performed:

- 241 1) MISDc model has been calibrated over the entire 2007-2016 period by using as input the
242 mean areal E-OBS rainfall and air temperature data for each basin; these simulated
243 discharge data, Q_{E-OBS} , has been used as benchmark to estimate the accuracy of the selected
244 SRPs for river discharge simulation.
- 245 2) MISDc has been run for each basin by using as input the mean areal SRPs and E-OBS air
246 temperature data. In accordance with literature studies (e.g, Thiemig et al., 2013), in these
247 runs the model parameters are calibrated separately for each SRP. The period 2007-2012 is



248 used for the parameter values calibration, whereas the remaining 2013-2016 period is used
 249 for the validation; Q_{E-OBS} is used as reference for parameter values calibration.

250

251 The use of Q_{E-OBS} as benchmark presents three advantages as it allows: 1) to consider a common
 252 and extended analysis period for all basins, 2) to consider a common benchmark in evaluating the
 253 SRP accuracy both in terms of rainfall and in terms of discharge and, more important, 3) to neglect
 254 the uncertainty due to the hydrological model structure in the SRPs comparison.

255 4.5 Performance metrics

256 The quality assessment of the different SRPs has been calculated by four continuous dimensionless
 257 metrics and three categorical scores. Among the continuous scores, the Pearson correlation
 258 coefficient, R , the relative BIAS, $rBIAS$, the relative root mean square error, $RRMSE$ and the KGE,
 259 an index increasingly used in hydrology to measure the goodness-of-fit between simulated and
 260 observed data, have been computed between the daily E-OBS and the satellite rainfall data averaged
 261 over the area of each basin as follows:

$$262 \quad R = \frac{\text{Cov}(SRP, P_{ref})}{\sigma_{SPR} \times \sigma_{P_{ref}}} \quad (1)$$

$$263 \quad rBIAS = \frac{\frac{1}{n} \sum_{i=1}^n (SRP_i - P_{ref_i})^2}{\frac{1}{n} \sum_{i=1}^n (P_{ref_i})^2} \quad (2)$$

$$264 \quad RRMSE = \frac{\sqrt{\frac{1}{n} \sum_{i=1}^n (SRP_i - P_{ref_i})^2}}{\frac{1}{n} \sum_{i=1}^n (P_{ref_i})} \quad (3)$$

$$265 \quad KGE = 1 - \sqrt{(R - 1)^2 + \left(\frac{\frac{1}{n} \sum_{i=1}^n (SRP_i)}{\frac{1}{n} \sum_{i=1}^n (P_{ref_i})} - 1 \right)^2 + \left(\frac{\frac{1}{n} \sum_{i=1}^n (P_{ref_i}) * \sigma_{SPR}}{\frac{1}{n} \sum_{i=1}^n (SRP_i) \sigma_{P_{ref}}} - 1 \right)^2} \quad (4)$$

266

267 where SRP and P_{ref} represent the SRPs and E-OBS rainfall time series; Cov and σ are the
 268 covariance and the standard deviation operator, respectively; n corresponds to the length of the time
 269 series. R values range from -1 to 1; $rBIAS$ ranges from $-\infty$ to $+\infty$; $RRMSE$ is bounded from 0 to $+\infty$
 270 while KGE varies between $-\infty$ to 1. More R , $rBIAS$, $RRMSE$ and KGE values goes toward 1, 0, 0,



271 1 respectively, higher is the agreement between E-OBS and SRPs. In particular, for KGE, model
272 performance in the range $-0.41 < KGE \leq 1$ indicate that the model outperforms the mean of the
273 observations (Knoben et al., 2019). In addition, for each SRP and for different rainfall thresholds
274 three categorical metrics are evaluated (Chen et al., 2012, Brocca et al., 2014): probability of
275 detection (POD), false alarm ratio (FAR) and threat score (TS) POD reports on the capability of
276 SRP to correctly detect rainfall events, FAR counts the fraction of rainfall events that are actually
277 non-events and TS takes into account the correctly detected, missed rainfall events and false
278 alarms.. These categorical metrics range from 0 to 1: higher POD and TS along with lower FAR
279 values indicate a better capability of SRPs to detect rainfall events.

280 To evaluate the suitability of rainfall products for flood modelling, the KGE index between the
281 observed and simulated discharge data has been computed. Specifically, KGE index has been
282 evaluated both between the observed and simulated Q_{E-OBS} discharge and between Q_{E-OBS} and the
283 simulated discharge data obtained by using SRPs as input, in order to establish the hydrological
284 performances of E-OBS and SRPs, respectively. Discharge simulations characterized by KGE
285 values greater than 0.5 have been considered good with respect to their ability to reproduce
286 observed discharge time series (Thiemig et al., 2013).

287 **5. RESULTS**

288 The findings of this work for the three SRPs are presented below. The SRP quality has been
289 evaluated first in terms of rainfall and then in terms of discharge. The propagation of the rainfall
290 error into the discharge simulation has been finally investigated.

291 **5.1 Rainfall assessment**

292 The performances of the three SRPs against the E-OBS datasets are illustrated in Figure 2. For sake
293 of brevity, the SRPs performances are presented only for the validation period (2013-2016), but
294 similar findings are obtained in the calibration period (see Table 3). Specifically, rBIAS, R,
295 RRMSE and KGE values are illustrated in the rows of Figure 2 for each study basin, for the three



296 products TMPA, CMOR and SM2R_{ASCAT} in each column. At the top of each plot, the median score
297 value is reported by considering the original spatial coverage of each SRP whereas in Table 3 the
298 performances of the basins whose outlet section is located below/above 50° latitude, i.e.
299 below/above the TMPA coverage, are listed. Already at first glance, it is possible to note that the
300 three products show similar patterns in terms of R and RRMSE whereas the same does not hold for
301 the rBIAS and KGE. By focusing the analysis over the TMPA area, median R (RRMSE) values are
302 equal to 0.626 (1.968), 0.551 (1.969), 0.609 (1.781) for TMPA, CMOR and SM2R_{ASCAT},
303 respectively. Higher/lower R/RRMSE values are obtained in Central Europe; the opposite is
304 observed in the Mediterranean area. The rBIAS is low for TMPA and SM2R_{ASCAT}, with median
305 values equal to -0.127 and 0.081, respectively, whereas CMOR show a clear underestimation of the
306 daily rainfall data over the entire European area. In terms of KGE, TMPA presents higher values
307 with respect to the other two products above all over the basins whose outlet section is located
308 between 40° and 50° latitude. Median KGE value for TMPA is equal to 0.516; this value reduces of
309 about 24% and 42% for SM2R_{ASCAT} and CMOR, respectively.

310 Outside the TMPA area and until 60° latitude, CMOR and SM2R_{ASCAT} show quite similar
311 performances in terms of R and RRMSE, while SM2R_{ASCAT} outperforms CMOR in terms of rBIAS
312 and KGE. Likely due to soil freezing and snow presence, the performances of SM2R_{ASCAT} decrease
313 in terms of R, rBIAS and KGE moving toward northern Europe (Brocca et al., 2019).

314 Results in terms of categorical metrics are summarized in Figure S1, where POD (first row), FAR
315 (second row) and TS (third row) have been computed for the validation period for three rainfall
316 thresholds (0.5, 5, and 10 mm/day) in order to assess the capability of SRPs to detect low to high
317 rainfall events. Numbers at the top of each plot represent the median score value obtained by
318 considering the original spatial coverage of each product. For all the three metrics and for moderate
319 to heavy rainfall events, TMPA presents the highest values of POD (median values equal to
320 0.500/0.415 for moderate/high events) and TS (median values equal to 0.368/0.288 for
321 moderate/high events), overperforming the other two products. Conversely, SM2R_{ASCAT} show



322 higher ability to detect small and moderate rainfall events with performances in terms of TS slightly
323 lower than the ones of TMPA product.

324 **5.2 Discharge assessment**

325 Prior to assess the hydrological performances of the satellite rainfall data, MISDc model has been
326 run with the E-OBS rainfall data as input to obtain Q_{E-OBS} , the benchmark river discharge data. The
327 results of this calibration, carried out for the entire observation period (2007-2016), are good as
328 illustrated in Figure 1b: the median KGE value obtained for the European area is equal to 0.768
329 (0.770 over the TMPA area). This ensures the good quality of Q_{E-OBS} data that are assumed as
330 benchmark for the successive analysis. Hereinafter, the hydrological performance has been assessed
331 in terms of KGE with respect to Q_{E-OBS} , with values higher than 0.5 considered as good.

332 Depending on the product, SRPs show different hydrological performances as illustrated in Figure 3
333 for the validation period and in Table 4 for both the calibration and the validation periods. At the
334 top of each plot in Figure 3, the median KGE value, averaged over the spatial coverage of each
335 product, is reported whereas in Table 4 the performances of the basins whose outlet section is
336 located below/above 50° latitude are listed. In addition, in Table 4 the percentage of basins showing
337 KGE values higher than 0.5 is computed.

338 By averaging the performances over the spatial coverage of each product, median KGE values
339 range from 0.279 to 0.722 for CMOR and SM2R_{ASCAT}, respectively, in the calibration period and
340 from -0.090 to 0.569 for the same products in the validation period (Figure 3). The percentage of
341 the basins showing KGE values higher than 0.5, is 88% and 18% for CMOR and SM2R_{ASCAT},
342 respectively, whereas the same percentage drop in the validation period up to about 39% and 3% for
343 the same products. TMPA is in the middle between the two products in terms of performances; the
344 percentage of basins with good hydrological performances is similar to the one of SM2R_{ASCAT}.

345 Similar findings hold if the comparison is carried out below the TMPA area (see Table 4): poor
346 results are obtained by CMOR during the validation period (median KGE<0; only 2.6% show KGE
347 higher than 0.5), whereas SM2R_{ASCAT} outperforms TMPA in both periods. In particular, during the



348 validation, period a median KGE value equal to 0.580 is obtained for SM2R_{ASCAT} against a value
349 equal to 0.428 for TMPA. Moreover, by comparing SM2R_{ASCAT} against TMPA in terms of basins
350 with KGE greater than 0.5, the ratio is two to one, i.e., 64% of basins show good hydrological
351 performances when forced with SM2R_{ASCAT} with respect to 39% for TMPA. The lowest
352 performances for both products are obtained over southern Spain and northern Italy. Conversely,
353 the basins located over northern Spain and central Europe show a better agreement with respect to
354 Q_{E-OBS} benchmark data, above all when SM2R_{ASCAT} is used as rainfall input. The performances of
355 SM2R_{ASCAT} remain good also when the analysis is extended above the TMPA area, with a median
356 KGE higher than 0.5 (Table 4). This is the first notably result of the paper, i.e., among the SRPs
357 available in near real time, there are some products that can be reasonably used to force a
358 hydrological model in order to obtain reliable discharge data over Europe. However, a question
359 remains: why do some SRPs perform better than others? Is it possible to find a rainfall score to
360 select a priori the best SRP to obtain reliable discharge simulations? Is there any link between
361 rainfall and discharge performances? The answer to these questions is given in the next paragraph
362 where the rainfall performances are compared with the discharge performances.

363 **5.3 Rainfall vs discharge performances**

364 By comparing the patterns of Figure 2 against the patterns of Figure 3, some insights about the link
365 between the rainfall accuracy and the hydrological performance can be noted: the basins with the
366 highest RRMSE (e.g., in the Mediterranean area and in particular in southern Spain and northern
367 Italy) correspond to basins with poorer hydrological performances ($KGE < 0.4$). In addition, as
368 occurs for CMOR product, high rBIAS values (both negative or positive) produce negative KGE
369 values. Interestingly, R and KGE rainfall scores seem to be weakly linked to the hydrological
370 performances. Finally, no clear link can be highlighted between KGE of discharge and the rainfall
371 categorical scores as for instance, the high/low values of SM2R_{ASCAT} in terms of FAR/TS do not
372 explain the higher performances of this products in terms of discharge (see Figure 3 against Figure
373 S1).



374 To better investigate these relationships, the scatterplots of Figure 4 and Figure S2 (in the
375 supplementary material) have been constructed for the continuous and categorical scores,
376 respectively. For each basin and for each SRP, the rainfall scores (x-axis) are plotted against the
377 KGE values (y-axis), resulting in a large ensemble of points spread out in the full range of
378 rainfall/discharge scores without any apparent relationship. The unique remark from Figure 4 is that
379 CMOR shows higher rBIAS and lower KGE values with respect to the other two products; rBIAS
380 of SM2R_{ASCAT} varies near zero and, in terms RRMSE, SM2R_{ASCAT} is characterized by a reduced
381 range of variability, (i.e., most of the SM2R_{ASCAT} data are characterized by RRMSE ranging from
382 1.5 and 2.5) with respect to the other two products. By looking at the categorical scores (Figure S2),
383 the three products show a similar variability range for moderate to high rainfall events whereas
384 some differences are evident for low rainfall events, that however should have a minor impact on
385 flood modelling. In particular, SM2R_{ASCAT} tend to have higher POD values for rainfall threshold
386 equal to 0.5, due to the tendency of the product to overestimate the rainfall occurrence (Brocca et
387 al., 2019).

388 To extract useful information from Figure 4 and Figure S2, the scores obtained separately for each
389 product have been grouped and the KGE data points have been binned into uniform ranges (with
390 step 0.1) of rainfall scores. The median KGE, and the 25th and 75th percentiles of KGE values, have
391 been computed for each rainfall score within each bin. The white dots in Figure 4 and Figure S2
392 represent, for each bin of each rainfall score, the median KGE value, the two ends of the black lines
393 in the same figure represent the 25th and 75th percentile of the KGE data points. By looking at the
394 boxplots so obtained, some insights already anticipated by inspecting Figure 2 versus Figure 3 for
395 the continuous scores can be confirmed: SRP hydrological performances strongly decrease by
396 increasing the absolute value of rBIAS, |rBIAS|, and the RRMSE values (Figure 4a and b) whereas
397 KGE of discharge slightly increase with R and KGE of rainfall (Figure 4c and d). If these
398 relationships have reflected the expectations, the same did not occur for the categorical scores.
399 Indeed, except for the rainfall threshold equal to 10 mm/day, the relationships between KGE of



400 discharge and the categorical scores of small and moderate rainfall are different (and sometimes
401 inverse) from what can be expected. This could be due to the lowest impact of small/moderate
402 rainfall events on flood generation. Then, focusing the attention only on high rainfall events, seems
403 that KGE of discharge slightly increase with POD whereas a stronger link can be noted between
404 KGE of discharge and FAR/TS.

405 The findings obtained so far become even more interesting if the following question is posed: for
406 which values of rainfall scores is it possible to obtain good results in terms of river discharge
407 simulation (i.e., $KGE > 0.5$ evaluated on the discharge data)? The straight grey line in Figure 4 (and
408 Figure S2), drawn for a threshold value of KGE equal to 0.5, helps us to answer the question
409 suggesting that good hydrological performances can be obtained for SRPs characterized by rBIAS
410 values close to 0 and small RRMSE scores. Conversely, R and KGE of rainfall seem to have a small
411 impact on KGE of discharge as for a large range of R and KGE values (from 0.5 to 0.8 and from 0.4
412 to 0.8, respectively), it is possible to obtain high KGE values. Similar conclusions hold for the
413 categorical scores evaluated for heavy rainfall events: the higher capability of SRPs to detect
414 rainfall events does not affect the hydrological performances, i.e., it is possible to obtain KGE of
415 discharge higher than 0.5 for a large range of POD, FAR and TS values. A further question remains:
416 how small/large should be the rainfall scores to obtain good hydrological performances, i.e., KGE
417 greater than 0.5? In particular, what about rBIAS and RRMSE that seem to have a stronger link
418 with the hydrological performances?

419 The boxplot of Figure 5a shows the hydrological performances that have been obtained during the
420 validation period by the three SRPs without any constrain on the rainfall scores. In order to consider
421 always the same number of basins for all the products, the area of analysis is cut below the TMPA
422 area and a median KGE value equal to 0.342 is obtained for the 889 basins. According to Table 4,
423 nearly 35% of the basins show KGE greater than 0.5. If the absolute value of rBIAS, |rBIAS|, is
424 constrained to values lower than 0.2 (Figure 5b), the median KGE value over the 400 basins that
425 fulfil the criteria is equal to 0.525. As shown in Figure 5c, a constrain on RRSME lower than 2 is



426 not enough to assure good hydrological performances (median KGE lower than 0.5) whereas if a
427 combination of the two rainfall scores is considered, the threshold on $KGE > 0.5$ is exceeded by
428 nearly 75% of the basins fulfilling the criteria (see first boxplot of Figure 5d). In other words, it
429 means that nearly less than 25% of the basins fulfilling the criteria shows low performance (first
430 boxplot of Figure 5d). Alternatively, less than 25% of basins not fulfilling the rainfall constrains
431 shows good hydrological performances (see second boxplot of Figure 5d).

432 For completeness of the work, a figure similar to Figure 5 has been added in the Supplementary
433 material (Figure S3) for the other rainfall scores (R, KGE, POD, FAR and TS and relative
434 combinations), but no one of the shown rainfall constrain can be considered satisfactory for the
435 analysis purpose. Indeed, no one of the rainfall constrain in Figure S3 allows a clear separation
436 between basins fulfilling/not fulfilling the criteria with a corresponding increase of KGE on
437 discharge.

438 6. DISCUSSION

439 The findings of Figure 4 and Figure 5 draw some interesting conclusions about the main research
440 question of the paper, i.e., for which rainfall metric it is possible to obtain good results in terms of
441 river discharge simulation. rBIAS along with RRMSE seem to be the most appropriate error metrics
442 to be used in conjunction to select the best performing SRP for flood modelling. With respect to
443 bias, the finding is in line with literature studies. For instance, Maggioni et al., (2013) showed that
444 bias can double from rainfall to runoff consistently from small to large basins. Conversely, no
445 suggestions can be found with respect to RRMSE or R metrics to characterize the SRPs potentiality
446 in terms of flood modelling. In the scientific literature, we have found thresholds on metric scores to
447 express the quality of SRPs in terms of rainfall. In particular, some authors considered an R value
448 equal or greater than 0.7 (Condom et al., 2011), a normalized RMSE values less than or equal to 0.5
449 (Adeyewa and Nakamura, 2003, Condom et al., 2011; Satgé et al., 2016; Shrestha et al., 2017) and



450 bias ranging from $-10\% \leq \text{bias} \leq 10\%$ (Brown, 2006, Yang and Luo, 2014) to be associated with
451 good satellite rainfall performances, but without a reference to justify these numbers.
452 Specifically, in this study we have found that constraining $|\text{rBIAS}|$ to values lower than 0.2 and
453 RRMSE to values lower than 2, good hydrological performances are assured for nearly 75% of the
454 basins fulfilling the criteria. The remaining percentage of basins for which the rainfall/discharge
455 performance relationship is not satisfied highlights that it is not straightforward to find such kind of
456 relationships as errors on rainfall and discharge data used as benchmark as well as the hydrological
457 model recalibration could influence the analysis. These findings corroborate those obtained by Qi et
458 al. (2016), stating that a good discharge simulation is a results of a good combination between a
459 rainfall product and an hydrological model, and the selection of the most accurate rainfall product
460 alone does not guarantee the most accurate hydrological performances.

461 7. CONCLUSIONS

462 This study represents the most comprehensive European-scale evaluation to date of satellite rainfall
463 products (SRPs). Three different near real time SRPs are used to force a lumped hydrological model
464 over 1318 basins throughout Europe. The results can be summarized as follows:

- 465 1. In terms of rainfall accuracy, the three SRPs show similar patterns in terms of R and
466 RRMSE whereas the same does not hold for the rBIAS. For the three products,
467 higher/lower R/RRMSE values are obtained in Central Europe; the opposite, is observed in
468 the Mediterranean area. The rBIAS is low for TMPA and SM2R_{ASCAT}, whereas CMOR
469 shows a clear underestimation of the daily rainfall data over the entire European area.
- 470 2. Among the SRPs available in near real time, there are some SRPs that can be reasonably
471 used to force a hydrological model in order to obtain reliable discharge data over Europe. In
472 particular, SM2R_{ASCAT} is the best performing product for flood simulation across Europe
473 (even at high latitudes).



474 3. There is a link between rainfall accuracy and discharge performance. In particular, by
475 constraining $|\text{rBIAS}|$ to values lower than 0.2 and RRMSE to values lower than 2, good
476 hydrological performances are assured for almost 75% of the basins fulfilling these criteria.

477

478 Overall, we believe the results obtained from this study provide very useful information about the
479 application of SRPs to simulate river discharge at basin scale. In particular, for the first time, this
480 work has addressed the topic of providing quantitative guidelines in the use of SRPs for near real
481 time hydrological applications.

482 Nevertheless, some limitations can be recognized in the analysis. One of the main limitations lies in
483 the use of only one hydrological model for flood simulation. In this respect, further analysis with
484 multiple hydrological models will be carried out to better investigate the link between rainfall,
485 hydrological model and discharge performances. In addition, in future researches the rainfall
486 metrics ranges here defined will be checked also with the use of different satellite rainfall products
487 (e.g., the Global Precipitation Measurement, GPM, Huffmann et al., 2018) and in different regions
488 worldwide. In particular, the extension of the analysis over different regions in the world could
489 allow to explore the connection between rainfall accuracy and discharge performances as a function
490 of additional criteria such as climate type, soil characteristics and terrain features (topography).

491 Another limitation of the study relies in having considered only one performance score for the
492 discharge. Indeed, as the main purpose of this study has been to reproduce the entire discharge time
493 series, any special attention to high/low flows was not paid. In a further analysis, a more
494 comprehensive study could consider a larger set of discharge metrics to better address the SRP
495 selection. Finally, the results of this study are likely sensitive to the quality of data taken as
496 “reference”, i.e., the E-OBS datasets, used as benchmark to evaluate the performances of SRPs both
497 in terms of rainfall and, through the hydrological model, in terms streamflow.



498 Despite the aforementioned limitations this study, contributing in the purpose of better understand
499 the propagation of the satellite rainfall error to streamflow simulations, could be very helpful for
500 data users facing the selection of the best satellite rainfall for hydrological applications.

501 **Author contribution**

502 S.C. collected discharge data, performed the analysis and wrote the manuscript. L.C. collected
503 satellite rainfall data; I.M. performed the basins delineation; C.M. and L.B. contributed on the
504 supervision of the work. All authors discussed the results and contributed to the final manuscript.

505 **Competing interests**

506 The authors declare that they have no conflict of interest.

507 **Acknowledgments**

508 The authors wish to thank the Global Runoff Data Centre (GRDC) for providing most of the
509 streamflow data throughout Europe and the E-OBS dataset from the EU-FP6 project UERRA
510 (<http://www.uerra.eu>) and the Copernicus Climate Change Service, and the data providers in the
511 ECA&D project (<https://www.ecad.eu>). The authors gratefully acknowledge support from
512 EUMETSAT through the “Satellite Application Facility on Support to Operational Hydrology and
513 Water Management (H SAF)” CDOP3 (EUM/C/85/16/DOC/15) and the Global SM2RAIN project
514 (contract n° EUM/CO/17/4600001981/BBo), and from ESA through SMOS+rainfall project
515 (contract n° 4000114738/15/I-SBo).

516



517 **REFERENCE**

- 518 Adeyewa, Z. D., & Nakamura, K. (2003). Validation of TRMM radar rainfall data over major climatic regions in
519 Africa. *Journal of Applied Meteorology*, 42(2), 331-347.
- 520 Artan, G., Gadain, H., Smith, J. L., Asante, K., Bandaragoda, C. J., & Verdin, J. P. (2007). Adequacy of satellite
521 derived rainfall data for stream flow modeling. *Natural Hazards*, 43(2), 167-185.
- 522 Beck, H. E., Vergopolan, N., Pan, M., Levizzani, V., Van Dijk, A. I., Weedon, G. P., ... & Wood, E. F. (2017). Global-
523 scale evaluation of 22 precipitation datasets using gauge observations and hydrological modeling. *Hydrology and*
524 *Earth System Sciences*, 21(12), 6201-6217.
- 525 Berghuijs, W. R., Harrigan, S., Molnar, P., Slater, L. J., & Kirchner, J. W. (2019). The relative importance of different
526 flood-generating mechanisms across Europe. *Water Resources Research*.
- 527 Bhuiyan, E., Abul, M., Nikolopoulos, E. I., Anagnostou, E. N., Polcher, J., Albergel, C., ... & Munier, S. (2019).
528 Assessment of precipitation error propagation in multi-model global water resource reanalysis. *Hydrology and Earth*
529 *System Sciences*, 23(4), 1973-1994.
- 530 Bisselink, B., Zambrano-Bigiarini, M., Burek, P., & De Roo, A. (2016). Assessing the role of uncertain precipitation
531 estimates on the robustness of hydrological model parameters under highly variable climate conditions. *Journal of*
532 *Hydrology: Regional Studies*, 8, 112-129.
- 533 Bitew, M. M., & Gebremichael, M. (2011). Evaluation of satellite rainfall products through hydrologic simulation in a
534 fully distributed hydrologic model. *Water Resources Research*, 47(6).
- 535 Brocca, L., Melone, F., Moramarco, T. (2011). Distributed rainfall-runoff modelling for flood frequency estimation and
536 flood forecasting. *Hydrological Processes*, 25 (18), 2801-2813, doi:10.1002/hyp.8042.
- 537 Brocca, L., Liersch, S., Melone, F., Moramarco, T., Volk, M. (2013a). Application of a model-based rainfall-runoff
538 database as efficient tool for flood risk management. *Hydrology and Earth System Sciences*, 17, 3159-3169,
539 doi:10.5194/hess-17-3159-2013.
- 540 Brocca, L., Moramarco, T., Dorigo, W., & Wagner, W. (2013b). Assimilation of satellite soil moisture data into
541 rainfall-runoff modelling for several catchments worldwide. In 2013 IEEE International Geoscience and Remote
542 Sensing Symposium-IGARSS (pp. 2281-2284). IEEE.
- 543 Brocca, L., Ciabatta, L., Massari, C., Moramarco, T., Hahn, S., Hasenauer, S., Kidd, R., Dorigo, W., Wagner, W.,
544 Levizzani, V. (2014). Soil as a natural rain gauge: estimating global rainfall from satellite soil moisture data. *Journal*
545 *of Geophysical Research*, 119(9), 5128-5141, doi:10.1002/2014JD021489.
- 546 Brocca, L., Filippucci, P., Hahn, S., Ciabatta, L., Massari, C., Camici, S., Schüller, L., Bojkov, B., Wagner, W. (2019).
547 SM2RAIN-ASCAT (2007-2018): global daily satellite rainfall from ASCAT soil moisture. *Earth System Science*
548 *Data Discussion*, under review, doi:10.5194/essd-2019-48. <https://doi.org/10.5194/essd-2019-48>.
- 549 Brown, J. E. (2006). An analysis of the performance of hybrid infrared and microwave satellite precipitation algorithms
550 over India and adjacent regions. *Remote Sensing of Environment*, 101(1), 63-81.
- 551 Camici, S., Brocca, L., Melone, F., Moramarco, T. (2014). Impact of climate change on flood frequency using different
552 climate models and downscaling approaches. *Journal of Hydrologic Engineering*, 19(8), 04014002,
553 doi:10.1061/(ASCE)HE.1943-5584.0000959. [http://dx.doi.org/10.1061/\(ASCE\)HE.1943-5584.0000959](http://dx.doi.org/10.1061/(ASCE)HE.1943-5584.0000959)
- 554 Camici, S., Ciabatta, L., Massari, C., and Brocca, L. (2018). How reliable are satellite precipitation estimates for driving
555 hydrological models: a verification study over the Mediterranean area. *Journal of Hydrology*, 563, 950-961.
- 556 Casse, C., Gosset, M., Peugeot, C., Pedinotti, V., Boone, A., Tanimoun, B. A., & Decharme, B. (2015). Potential of
557 satellite rainfall products to predict Niger River flood events in Niamey. *Atmospheric Research*, 163, 162-176.
- 558 Chen, F., Crow, W., & Holmes, T. R. (2012). Improving long-term, retrospective precipitation datasets using satellite
559 surface soil moisture retrievals and the soil moisture analysis rainfall tool. *Journal of Applied Remote Sensing*, 6(1),
560 063604.



- 561 Chintalapudi, S., Sharif, H., & Xie, H. (2014). Sensitivity of distributed hydrologic simulations to ground and satellite
562 based rainfall products. *Water*, 6(5), 1221-1245.
- 563 Cislaghi, A., Masseroni, D., Massari, C., Camici, S., Brocca, L. (2019). Combining rainfall-runoff model and
564 regionalization approach for flood and water resource assessment in the western Po-Valley (Italy). *Hydrological
565 Science Journal*, in press, doi:10.1080/02626667.2019.1690656.
- 566 Condom, T., Rau, P., & Espinoza, J. C. (2011). Correction of TRMM 3B43 monthly precipitation data over the
567 mountainous areas of Peru during the period 1998–2007. *Hydrological Processes*, 25(12), 1924-1933.
- 568 Cornes, R. C., van der Schrier, G., van den Besselaar, E. J., & Jones, P. D. (2018). An Ensemble Version of the E-OBS
569 Temperature and Precipitation Data Sets. *Journal of Geophysical Research: Atmospheres*, 123(17), 9391-9409.
- 570 Demaria, E. M., Nijssen, B., Valdés, J. B., Rodriguez, D. A., & Su, F. (2014). Satellite precipitation in southeastern
571 South America: how do sampling errors impact high flow simulations?. *International journal of river basin
572 management*, 12(1), 1-13.
- 573 Ebert, E. E., Janowiak, J. E., & Kidd, C. (2007). Comparison of near-real-time precipitation estimates from satellite
574 observations and numerical models. *Bulletin of the American Meteorological Society*, 88(1), 47-64.
- 575 Elgamal, A., Reggiani, P., & Jonoski, A. (2017). Impact analysis of satellite rainfall products on flow simulations in the
576 Magdalena River Basin, Colombia. *Journal of Hydrology: Regional Studies*, 9, 85-103.
- 577 Gebregiorgis, A. S., Tian, Y., Peters-Lidard, C. D., & Hossain, F. (2012). Tracing hydrologic model simulation error as
578 a function of satellite rainfall estimation bias components and land use and land cover conditions. *Water Resources
579 Research*, 48(11).
- 580 Gupta, H. V., Kling, H., Yilmaz, K. K., & Martinez, G. F. (2009). Decomposition of the mean squared error and NSE
581 performance criteria: Implications for improving hydrological modelling. *Journal of hydrology*, 377(1-2), 80-91.
- 582 Haylock, M. R., Hofstra, N., Klein Tank, A. M. G., Klok, E. J., Jones, P. D., & New, M. (2008). A European daily high-
583 resolution gridded data set of surface temperature and precipitation for 1950–2006. *Journal of Geophysical
584 Research: Atmospheres*, 113(D20).
- 585 Hong, Y., Hsu, K. L., Moradkhani, H., & Sorooshian, S. (2006). Uncertainty quantification of satellite precipitation
586 estimation and Monte Carlo assessment of the error propagation into hydrologic response. *Water resources research*,
587 42(8).
- 588 Hossain, F., & Anagnostou, E. N. (2006). A two-dimensional satellite rainfall error model. *IEEE transactions on
589 geoscience and remote sensing*, 44(6), 1511-1522.
- 590 Hossain, F., & Huffman, G. J. (2008). Investigating error metrics for satellite rainfall data at hydrologically relevant
591 scales. *Journal of Hydrometeorology*, 9(3), 563-575.
- 592 Huffman, G. J., Adler, R. F., Bolvin, D. T., & Nelkin, E. J. (2010). The TRMM multi-satellite precipitation analysis
593 (TMPA). In *Satellite rainfall applications for surface hydrology* (pp. 3-22). Springer, Dordrecht.
- 594 Huffman, G., Bolvin, D., Braithwaite, D., Hsu, K., Joyce, R., Kidd, C., Nelkin, E., and Xie, P. (2018). Algorithm
595 Theoretical Basis Document (ATBD) Version 4.5. NASA Global Precipitation Measurement (GPM) Integrated
596 Multi-satellitE Retrievals for GPM (IMERG) NASA.
- 597 Jiang, D., & Wang, K. (2019). The Role of Satellite Remote Sensing in Improving Simulated Streamflow: A Review.
598 *Water*, 11(8), 1615.
- 599 Joyce, R. J., Janowiak, J. E., Arkin, P. A., & Xie, P. (2004). CMORPH: A method that produces global precipitation
600 estimates from passive microwave and infrared data at high spatial and temporal resolution. *Journal of
601 Hydrometeorology*, 5(3), 487-503.
- 602 Kling, H., Fuchs, M., & Paulin, M. (2012). Runoff conditions in the upper Danube basin under an ensemble of climate
603 change scenarios. *Journal of Hydrology*, 424, 264-277.
- 604 Klok, E. J., and Tank, A. K. (2009). Updated and extended European dataset of daily climate observations. *International
605 Journal of Climatology*, 29(8), 1182-1191.



- 606 Knoben, W. J. M., Freer, J. E., and Woods, R. A. (2019). Technical note: Inherent benchmark or not? Comparing Nash-
607 Sutcliffe and Kling-Gupta efficiency scores, *Hydrol. Earth Syst. Sci. Discuss.*, [https://doi.org/10.5194/hess-2019-](https://doi.org/10.5194/hess-2019-327)
608 327, in review.
- 609 Lu, D.; Yong, B. (2018) Evaluation and Hydrological Utility of the Latest GPM IMERG V5 and GSMaP V7
610 Precipitation Products over the Tibetan Plateau. *Remote Sens.*, 10, 2022.
- 611 Maggioni, V., Reichle, R. H., & Anagnostou, E. N. (2011). The effect of satellite rainfall error modeling on soil
612 moisture prediction uncertainty. *Journal of Hydrometeorology*, 12(3), 413-428.
- 613 Maggioni, V., Vergara, H. J., Anagnostou, E. N., Gourley, J. J., Hong, Y., & Stampoulis, D. (2013). Investigating the
614 applicability of error correction ensembles of satellite rainfall products in river flow simulations. *Journal of*
615 *Hydrometeorology*, 14(4), 1194-1211.
- 616 Maggioni, V., Massari, C. (2018) On the performance of satellite precipitation products in riverine flood modeling: A
617 review. *Journal of Hydrology*, 558, 214-224.
- 618 Massari, C., Brocca, L., Ciabatta, L., Moramarco, T., Gabellani, S., Albergel, C., de Rosnay, P., Puca, S., Wagner, W.
619 (2015). The use of H-SAF soil moisture products for operational hydrology: flood modelling over Italy. *Hydrology*,
620 2(1), 2-22, doi:10.3390/hydrology2010002. <http://dx.doi.org/10.3390/hydrology2010002>
- 621 Massari, C., Camici, S., Ciabatta, L., Brocca, L. (2018). Exploiting satellite surface soil moisture for flood forecasting
622 in the Mediterranean area: state update versus rainfall correction. *Remote Sensing*, 10(2), 292, doi:
623 10.3390/rs10020292.
- 624 Masseroni, D., Cislaghi, A., Camici, S., Massari, C., & Brocca, L. (2016). A reliable rainfall-runoff model for flood
625 forecasting: review and application to a semi-urbanized watershed at high flood risk in Italy. *Hydrology Research*,
626 48(3), 726-740.
- 627 Mei, Y., Nikolopoulos, E., Anagnostou, E., Zoccatelli, D., & Borga, M. (2016). Error analysis of satellite precipitation-
628 driven modeling of flood events in complex alpine terrain. *Remote Sensing*, 8(4), 293.
- 629 Mei, Y., Anagnostou, E. N., Shen, X., & Nikolopoulos, E. I. (2017). Decomposing the satellite precipitation error
630 propagation through the rainfall-runoff processes. *Advances in water resources*, 109, 253-266.
- 631 Montani, A., Cesari, D., Marsigli, C., & Paccagnella, T. (2011). Seven years of activity in the field of mesoscale
632 ensemble forecasting by the COSMO-LEPS system: main achievements and open challenges. *Tellus A: Dynamic*
633 *Meteorology and Oceanography*, 63(3), 605-624.
- 634 Mouratidis, A., & Ampatzidis, D. (2019). European Digital Elevation Model Validation against Extensive Global
635 Navigation Satellite Systems Data and Comparison with SRTM DEM and ASTER GDEM in Central Macedonia
636 (Greece). *ISPRS International Journal of Geo-Information*, 8(3), 108. <https://doi.org/10.3390/ijgi8030108>
- 637 Mugnai, A., Casella, D., Cattani, E., Dietrich, S., Laviola, S., Levizzani, V., ... & Biron, D. (2013). Precipitation
638 products from the hydrology SAF. *Natural Hazards and Earth System Sciences*, 13(8), 1959-1981.
- 639 Nikolopoulos, E. I., Anagnostou, E. N., Hossain, F., Gebremichael, M., & Borga, M. (2010). Understanding the scale
640 relationships of uncertainty propagation of satellite rainfall through a distributed hydrologic model. *Journal of*
641 *Hydrometeorology*, 11(2), 520-532.
- 642 Nikolopoulos, E. I., E. N. Anagnostou, and M. Borga (2012). Using high-resolution satellite rainfall products to
643 simulate a major flash flood event in northern Italy. *J. Hydrometeor.*, 14, 171-185.
- 644 Pakoksung, K., and Takagi, M. (2016). Effect of satellite based rainfall products on river basin responses of runoff
645 simulation on flood event. *Modeling Earth Systems and Environment*, 2(3), 143.
- 646 Pan, M., Li, H., & Wood, E. (2010). Assessing the skill of satellite-based precipitation estimates in hydrologic
647 applications. *Water Resources Research*, 46(9).
- 648 Qi, W., Zhang, C., Fu, G., Sweetapple, C., & Zhou, H. (2016). Evaluation of global fine-resolution precipitation
649 products and their uncertainty quantification in ensemble discharge simulations. *Hydrology and Earth System*
650 *Sciences*, 20(2), 903-920.
- 651 Quintero, F., Krajewski, W. F., Mantilla, R., Small, S., & Seo, B. C. (2016). A spatial-dynamical framework for
652 evaluation of satellite rainfall products for flood prediction. *Journal of Hydrometeorology*, 17(8), 2137-2154.



- 653 Ren, P., Li, J., Feng, P., Guo, Y., & Ma, Q. (2018). Evaluation of multiple satellite precipitation products and their use
654 in hydrological modelling over the Luanhe River basin, China. *Water*, 10(6), 677.
- 655 Ricciardelli, E.; Di Paola, F.; Gentile, S.; Cersosimo, A.; Cimini, D.; Gallucci, D.; Gerdali, E.; Larosa, S.; Nilo, S.T.;
656 Ripepi, E.; et al. (2018). Analysis of Livorno Heavy Rainfall Event: Examples of Satellite Observation Techniques
657 in Support of Numerical Weather Prediction. *Remote Sens.*, 10, 1549.
- 658 Satgé, F., Bonnet, M. P., Gosset, M., Molina, J., Lima, W. H. Y., Zolá, R. P., ... & Garnier, J. (2016). Assessment of
659 satellite rainfall products over the Andean plateau. *Atmospheric research*, 167, 1-14.
- 660 Satgé, F., Ruelland, D., Bonnet, M. P., Molina, J., & Pillco, R. (2019). Consistency of satellite precipitation products in
661 space and over time compared with gauge observations and snow-hydrological modelling in the Lake Titicaca
662 region. *Hydrology and Earth System Sciences*, 23(1), 595-619.
- 663 Serpetzoglou, E., Anagnostou, E. N., Papadopoulos, A., Nikolopoulos, E. I., & Maggioni, V. (2010). Error propagation
664 of remote sensing rainfall estimates in soil moisture prediction from a land surface model. *Journal of*
665 *Hydrometeorology*, 11(3), 705-720.
- 666 Shah, H. L., & Mishra, V. (2016). Uncertainty and bias in satellite-based precipitation estimates over Indian
667 subcontinental basins: Implications for real-time streamflow simulation and flood prediction. *Journal of*
668 *Hydrometeorology*, 17, 615–636.
- 669 Shrestha, N. K., Qamer, F. M., Pedreros, D., Murthy, M. S. R., Wahid, S. M., & Shrestha, M. (2017). Evaluating the
670 accuracy of Climate Hazard Group (CHG) satellite rainfall estimates for precipitation based drought monitoring in
671 Koshi basin, Nepal. *Journal of Hydrology: Regional Studies*, 13, 138-151.
- 672 Tapiador, F.J.; Navarro, A.; Levizzani, V.; García-Ortega, E.; Huffman, G.J.; Kidd, C.; Kucera, P.A.; Kummerow,
673 C.D.; Masunaga, H.; Petersen, W.A.; et al. (2017). Global precipitation measurements for validating climate models.
674 *Atmos. Res.*, 197, 1–20.
- 675 Thiemig, V., Rojas, R., Zambrano-Bigiarini, M., & De Roo, A. (2013). Hydrological evaluation of satellite rainfall
676 estimates over the Volta and Baro-Akobo Basin. *Journal of Hydrology*, 499, 324-338.
- 677 Valdés-Pineda, R., Demaría, E. M., Valdés, J. B., Wi, S., & Serrat-Capdevila, A. (2016). Bias correction of daily
678 satellite rainfall estimates for hydrologic forecasting in the Upper Zambezi, Africa. *Hydrol. Earth Syst. Sci.*, 1, 28.
- 679 Vergara, H., Hong, Y., Gourley, J. J., Anagnostou, E. N., Maggioni, V., Stampoulis, D., & Kirstetter, P. E. (2014).
680 Effects of resolution of satellite rainfall estimates on hydrologic modeling skill at different scales. *Journal of*
681 *Hydrometeorology*, 15(2), 593-613.
- 682 Wagner, W., Hahn, S., Kidd, R., Melzer, T., Bartalis, Z., Hasenauer, S., ... & Komma, J. (2013). The ASCAT soil
683 moisture product: A review of its specifications, validation results, and emerging applications. *Meteorologische*
684 *Zeitschrift*, 22(1), 5-33.
- 685 Yang, Y., Luo, Y. (2014). Evaluating the performance of remote sensing precipitation products CMORPH,
686 PERSIANN, and TMPA, in the arid region of northwest China. *Theoretical and applied climatology*, 118(3), 429-
687 445.
- 688 Yilmaz, K. K., Hogue, T. S., Hsu, K. L., Sorooshian, S., Gupta, H. V., & Wagener, T. (2005). Intercomparison of rain
689 gauge, radar, and satellite precipitation estimates with emphasis on hydrologic forecasting. *Journal of*
690 *Hydrometeorology*, 6(4), 497-517.
- 691 Yong, B., Ren, L. L., Hong, Y., Wang, J. H., Gourley, J. J., Jiang, S. H., ... & Wang, W. (2010). Hydrologic evaluation
692 of Multisatellite Precipitation Analysis standard precipitation products in basins beyond its inclined latitude band: A
693 case study in Laohahe basin, China. *Water Resources Research*, 46(7).
- 694 Zappa, M., Rotach, M. W., Arpagaus, M., Dorninger, M., Hegg, C., Montani, A., ... & Jaun, S. (2008). MAP D-
695 PHASE: real-time demonstration of hydrological ensemble prediction systems. *Atmospheric Science Letters*, 9(2),
696 80-87.
- 697 Zhu, Q., Xuan, W., Liu, L., & Xu, Y. P. (2016). Evaluation and hydrological application of precipitation estimates
698 derived from PERSIANN-CDR, TRMM 3B42V7, and NCEP-CFSR over humid regions in China. *Hydrological*
699 *processes*, 30(17), 3061-3083.



700 Table 1. Main characteristics of the study basins clustered according to the latitude coordinate of the
701 outlet section.

| # | latitude | Number of basins | Median Area (km ²) | Median length of available discharge data after 2007 (years) |
|---|----------|------------------|--------------------------------|--|
| 1 | 35°- 50° | 889 | 800 | 8 |
| 2 | 50°- 60° | 288 | 960 | 7 |
| 3 | > 60° | 141 | 2484 | 8 |

702
703



704 Table 2. Main characteristics of the datasets used in this study.

| # | Satellite-only rainfall datasets | Spatial/ temporal resolution | Spatial coverage | Time period |
|---|--|------------------------------|--------------------------------|-------------|
| 1 | TMPA RT (3B42RT V7) | 0.25° / 3-hour | ±50° north-south latitude band | 2000 – 2018 |
| 2 | CMORPH | 0.25° /3-hour | ±60° north-south latitude band | 1998 – 2018 |
| 3 | SM2R _{ASCAT} | 0.25° / 24-hour | global, over land | 2007 – 2018 |
| # | Large scale gauge based rainfall dataset | Spatial/ temporal resolution | Coverage | Time period |
| 1 | E-OBS | 0.22° / 24-hour | Europe | 1950 – 2018 |
| # | Gauge based discharge dataset | Spatial/ temporal resolution | Coverage | Time period |
| 1 | European daily dataset | 1318 sites/daily | Europe | 1900 - 2016 |

705

706



707 Table 3. Performance scores for rainfall (in terms of rBIAS, R and RRMSE) time series computed
 708 during the calibration (in italic) and the validation periods. Rainfall performances are evaluated with
 709 respect to E-OBS rainfall data and distinguished between basins whose outlet section is below or
 710 above 50° latitude.

Rainfall performances

| Score | rBIAS | R | RRMSE | KGE | rBIAS | R | RRMSE | KGE |
|-----------------------|------------------------------------|------------------|------------------|------------------|-------------------------------------|------------------|------------------|------------------|
| | below TMPA area (latitude <50°) | | | | above TMPA area (latitude >=50°) | | | |
| Product | | | | | | | | |
| TMPA | -0.127 (-0.095) | 0.626 (0.619) | 1.968 (1.978) | 0.516 (0.533) | --- | --- | --- | --- |
| CMOR | -0.462 (-0.406) | 0.551 (0.576) | 1.969 (1.974) | 0.299 (0.375) | -0.635 (-0.618) | 0.544 (0.562) | 1.607 (1.621) | 0.114 (0.147) |
| SM2R _{ASCAT} | 0.081 (0.084) | 0.609 (0.595) | 1.781 (1.805) | 0.393 (0.436) | -0.086 (-0.080) | 0.572 (0.548) | 1.477 (1.514) | 0.331 (0.372) |

711

712

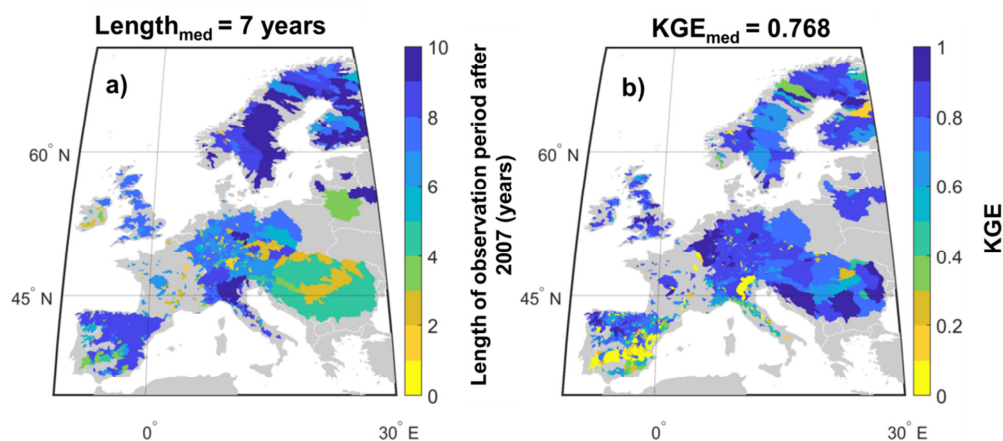


713 Table 4. Median KGE index computed by comparing Q_{E-OBS} simulated data against simulated
 714 discharge data obtained by forcing MISDc hydrological model with satellite (TMPA, CMOR,
 715 SM2R_{ASCAT}) rainfall data. Percentage of the basins showing KGE values higher than 0.5 is also
 716 listed. Performances and percentages are averaged over different spatial windows: the original
 717 spatial coverage of the product and below/above the TMPA area (latitude $\pm 50^\circ$).

| KGE | | | | | | |
|----------------------------|---------------------------------|-------------|--|-------------|---|-------------|
| Score | Spatial coverage of the product | | below TMPA area (latitude $< 50^\circ$) | | above TMPA area (latitude $\geq 50^\circ$) | |
| | cal | val | cal | val | cal | val |
| Product | | | | | | |
| TMPA | 0.692 | 0.428 | 0.692 | 0.428 | --- | --- |
| CMOR | 0.279 | -0.090 | 0.324 | -0.014 | 0.201 | -0.248 |
| SM2R _{ASCAT} | 0.722 | 0.569 | 0.751 | 0.580 | 0.670 | 0.539 |
| % of basins with KGE > 0.5 | | | | | | |
| TMPA | 87.9 | 38.6 | 87.9 | 38.6 | --- | --- |
| CMOR | 17.5 | 2.40 | 21.6 | 2.60 | 4.90 | 1.80 |
| SM2R _{ASCAT} | 87.6 | 61.7 | 92.6 | 64.0 | 77.2 | 56.9 |
| Average | 64.4 | 34.2 | 67.4 | 35.1 | 41.1 | 29.4 |

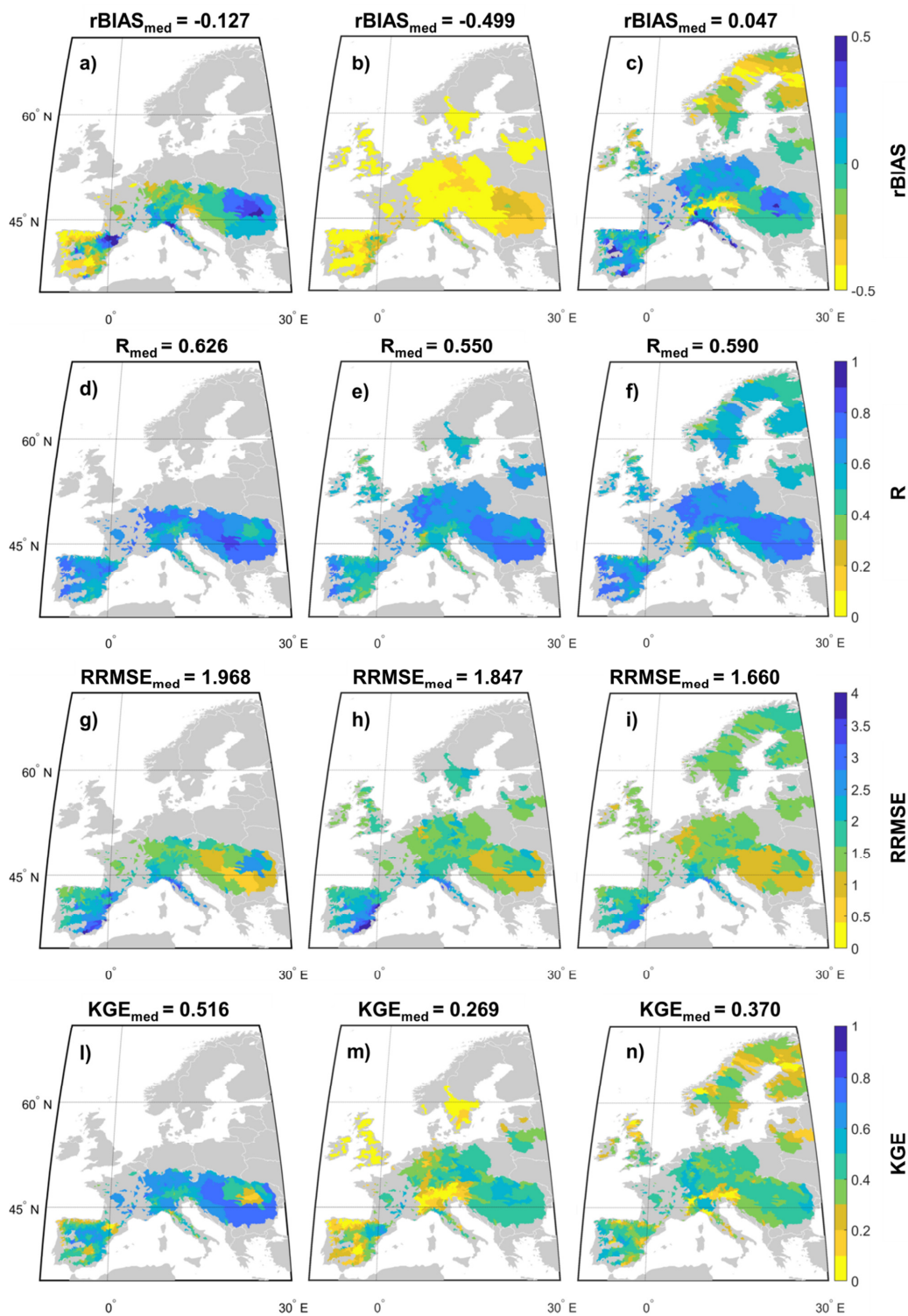
718

719



720

721 Figure 1. Location of study basins and a) length of discharge observation period after 2007; b) KGE
722 index obtained by comparing observed against modelled discharge data over the period 2007-2016.
723 Modelled data have been obtained by using E-OBS rainfall dataset as input to MISDc model.
724

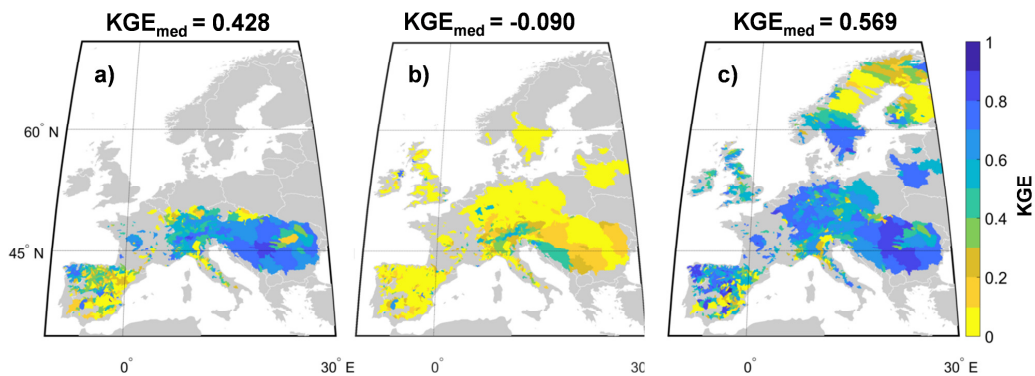




726 Figure 2. Performances of satellite rainfall during the validation period in terms of rBIAS (first
727 row), R (second row), RRMSE (third row), KGE (fourth row) over the study basins, for the three
728 products TMPA (first column), CMOR (second column) and SM2R_{ASCAT} (third column). Numbers
729 in each plot represent the median score value obtained by considering the original spatial coverage
730 of each product.
731



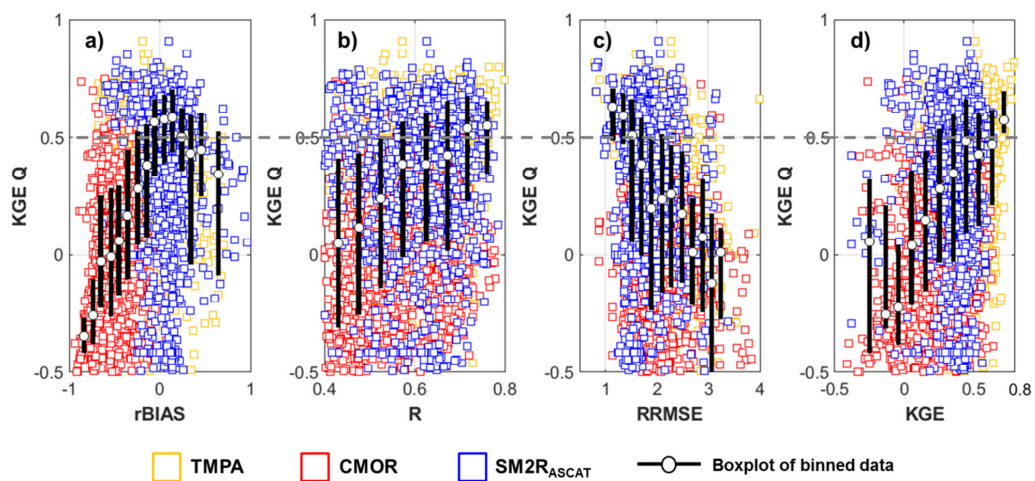
732



733

734 Figure 3. Maps of KGE index obtained by considering a, d) TMPA, b, e) CMORPH and c, f)
735 SM2R_{ASCAT} rainfall dataset in the validation period. In a), b) and c) plots, the median KGE value
736 averaged over the original product coverage is reported.

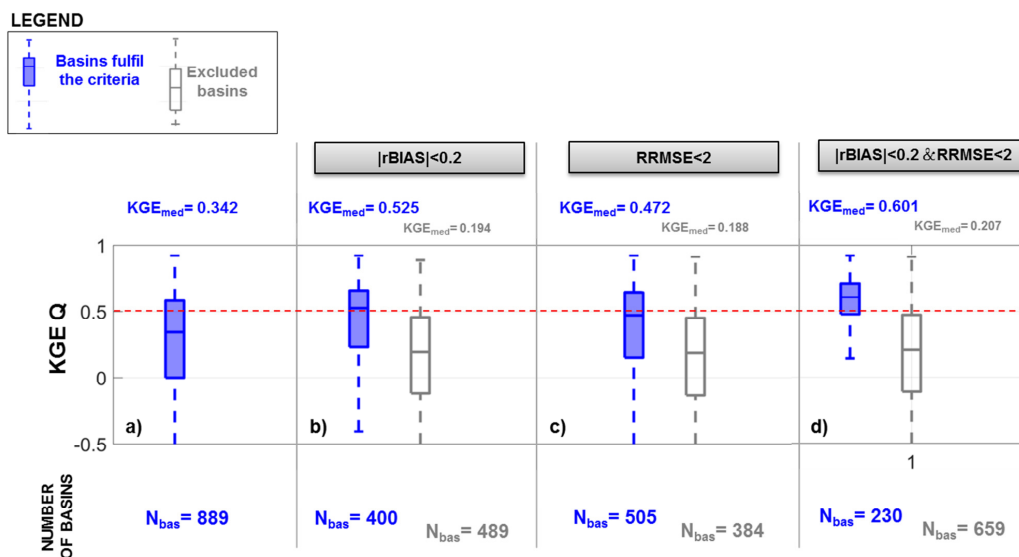
737



738

739 Figure 4. Performances of discharge in terms of KGE against a) relative rainfall bias, rBIAS; b)
740 rainfall correlation, R; c) relative root mean square error of rainfall, RRMSE, d) KGE of rainfall.
741 The scores are evaluated for the validation period (2013-2016) for all the 1318 basins.

742



743

746

Figure 5. Hydrological performances in terms of KGE values that can be obtained during the validation period by the three satellite rainfall products for all the basins whose outlet section is located below the TMPA area (889), a) without any constrain on the rainfall scores; b) constraining the module of rBIAS to values lower than 0.2; c) constraining RRMSE to values lower than 2; d) constraining the module of rBIAS to values lower than 0.2 and RRMSE to values lower than 2.

751

752

753